Dangling bonds and magnetism of grain boundaries in graphene

M. A. Akhukov,[1] A. Fasolino,[1] Y. N. Gornostyrev,[2] and M. I. Katsnelson[1]

[1]*Radboud University Nijmegen/Institute for Molecules and Materials, Heyendaalseweg 135, NL-6525AJ Nijmegen, The Netherlands*
[2]*Institute of Quantum Materials Science, Ekaterinburg 620175, Russian Federation*

Grain boundaries with dangling bonds (DBGB) in graphene are studied by atomistic Monte Carlo and molecular dynamics simulations in combination with density functional (SIESTA) calculations. The most stable configurations are selected and their structure is analyzed in terms of grain boundary dislocations. It is shown that the grain boundary dislocation with the core consisting of pentagon, octagon, and heptagon (5-8-7 defect) is a typical structural element of DBGB with relatively low energies. The electron energy spectrum and magnetic properties of the obtained DBGB are studied by density functional calculations. It is shown that the 5-8-7 defect is magnetic and that its magnetic moment survives after hydrogenation. The effects of hydrogenation and of out-of-plane deformations on the magnetic properties of DBGB are studied.

PACS number(s): 61.48.Gh, 73.22.Pr, 61.72.Mm, 75.75.−c

I. INTRODUCTION

Most potential applications of graphene require to construct macroscopically large samples that are bound to be polycrystalline. Several routes are currently actively pursued to obtain large samples in an efficient way. Examples are evaporation of surface layers of SiC,[1,2] solution of graphite without functionalization, in combination with sonication[3–5] to obtain graphene paper (laminate), and chemical vapor deposition on metals.[6,7] Studies of graphene grown by these methods confirm the existence of grain boundaries (GB), as was observed in graphene on SiC,[8] Ir(111),[9,10] polycrystalline Ni,[11] and Cu.[12] Although the presence of GB may be detrimental for electron mobility and mechanical strength, GB are potentially interesting by themselves, e.g., by metallicity along the grain as shown in Ref. 13. Several theoretical papers have considered the structure[14–17] and electronic[18] properties of tilt GB in graphene.

Grain boundaries were subject of intensive experimental and theoretical study in the 1970s. At that time, the basic principles of formation of GB structures were understood and the special class of GB characterized by high symmetry was identified by the coincidence-site-lattice (CSL) approach.[19] These GB have optimal matching of the grains and, being energetically the most favorable, are dominant in well-annealed polycrystalline samples. Most GB studied experimentally in graphene can indeed be classified as low-energy structures within the CSL theory.[7,17] These GB consist of regularly arranged dipoles of disclinations with rotation angles ±60° associated with five and sevenfold carbon rings.[14] The distance between disclination dipoles depends on the misalignment of the grains. The high strength characteristics of these GB in graphene[15] confirms the strong bonding in the core of the 5-7 disclination dipoles.

In bulk materials, however, less favorable GB with extrinsic structural defects, extra volume excess, and large elastic strain also have been observed, depending on the treatment of polycrystalline samples.[20] Also for graphene, one may expect this situation for samples obtained by coalescence of independently growing nuclei as typical of chemical vapor deposition. The properties of more general GB have been considered in Ref. 21, and in Ref. 16 it was shown that, in addition to 5-7 pairs, there are eightfold rings that dominate at a tilt angle close to 15° as well as four- and ninefold rings with less probability. In addition to having higher energy and excess free volume, these GB may also present dangling bonds and resemble structures found in amorphous graphene obtained by electron bombardment.[22]

The possibility of dangling bonds makes these high-energy GB particularly interesting since the dangling bonds can carry magnetic moments and are potential sources of magnetic ordering.[23] The possibility that grain boundaries can be a source of magnetism in graphitic materials was suggested in Ref. 24 based on the following experimental observations in highly oriented pyrolytic graphite (HOPG). Scanning tunneling microscope (STM) studies of GB with different periodicities found some peaks in the local density of states attributed to dangling bonds. Depending on the periodicity of the GB, these additional peaks in the density of states were either situated at the Fermi energy or split, which was interpreted as spin splitting. The room-temperature ferromagnetism measured by magnetic force microscopy and bulk magnetization measurements was tentatively attributed to two-dimensional magnetic ordering at the grain boundaries. The observation of room-temperature ferromagnetism was, however, not confirmed in other studies of HOPG.[25] Recently, a systematic study of samples of HOPG of different manufacturers[26] has convincingly attributed the macroscopic magnetic signal found in some of them to Fe-rich inclusions buried in the bulk. Nevertheless, the local STM data of Ref. 24 could still be related to the existence of localized magnetic moments and the possibility to achieve ferromagnetism in sp electron materials remains very appealing[27] and justifies further research.

In this paper, we study systematically the structural, electronic, and magnetic properties of GB with dangling bonds (DBGB) in graphene by a hierarchical approach based on classical atomistic simulations and *ab initio* calculations. As a result of a massive search based on simulated annealing by classical Monte Carlo simulations, we find that a particular structure with five, eight, and seven rings (5-8-7) appears to be kinetically stable up to high temperature and can be a common structural element of generic GB in graphene. According to

our DFT calculations the 5-8-7 defect contains one dangling bond with an associated magnetic moment of $\simeq 0.5$–1.0 μ_B with μ_B the Bohr magneton, that is only partially reduced by hydrogenation. This means that, in contrast to the low-energy GB, a generic GB in graphene and graphite can have unpaired electrons and magnetic moments. Note that, according to our calculations, the hydrogenation of DBGB turns out to be energetically favorable; thus, the most probably realistic DBGB in graphene should be passivated by hydrogen. At the same time, all qualitative conclusions about the structure and magnetism of GB do not depend on this assumption.

The paper is organized as follows. In Sec. II we present the methods for atomistic simulations and *ab initio* calculations. In Sec. III we describe the structure and energetics of DBGB in graphene and in Sec. IV we discuss their electronic structure and spin density. Finally, in Sec. V we give a summary and conclusions.

II. METHOD

A systematic study of GB is computationally demanding because it requires the examination of very large samples. Therefore, we have done a first search for DBGB by means of Monte Carlo simulations based on the classical long-range carbon bond-order potential II (LCBOPII) interatomic potential.[28] After having identified the 5-8-7 structure as a promising basic unit for DBGB, we have studied the electronic and magnetic properties by means of spin-polarized density functional theory (DFT) calculations as implemented in the SIESTA code. The drawing of flat pictures was done using the xyz2eps utility[29] written in the PYTHON programming language.[30] The visualization of 3D structures together with 3D charge density was done using the VESTA visualization program.[31]

A. Atomistic simulations with LCBOPII

The classical bond-order potential LCBOPII[28] has been shown to describe accurately the structure[32,33] and elastic properties[34] of graphene as well as the phonons,[35] the structure of the edges,[36] and bilayer graphene.[37] The accuracy of this potential for dealing with GB has been validated against DFT calculations in Ref. 17. For the present study, this potential has the important feature of being reactive, namely to allow breaking and formation of bonds as would happen when grains meet.

We have used Monte Carlo simulations in the NPT ensemble, that is, we have kept temperature T and number of particles N constant and allowed volume fluctuations to keep the pressure $P = 0$. To find (meta-)stable structures we have done a simulated annealing lowering the temperatures from 3300 K. The procedure to construct the samples is described in Sec. II C.

B. DFT *ab initio* calculations with the SIESTA code

We have performed spin-polarized DFT[38,39] calculations by means of the package SIESTA, which implements DFT on a localized basis set.[40–42] We used generalized gradient approximations with the Perdew-Burke-Ernzerhof parametrization (GGA-PBE)[43] and a standard built-in double-ζ polarized

(DZP)[44] basis set to perform geometry relaxation of graphene samples with GB. The DZP basis set represents core electrons by norm-conserving Troullier-Martins pseudopotentials[45] in the Kleynman-Bylander nonlocal form.[46] For a carbon atom this basis set has 13 atomic orbitals: a double-ζ for $2s$ and $2p$ valence orbitals and a single-ζ set of five d orbitals. The cutoff radii of the atomic orbitals were obtained from an energy shift equal to 0.02 Ry, which gives a cut-off radius of 2.22 Å for s orbitals and 2.58 Å for p orbitals. The real-space grid is equivalent to a plane-wave cutoff energy of 400 Ry, yielding ≈ 0.08 Å resolution for the sampling of real space. For nonperiodical directions, an extra space larger than 15 Å was added to avoid spurious interactions. We used k-point sampling of the Brillouin zone based on the Monkhorst-Pack scheme[47] where the number of k points was defined similarly to the k-grid cut-off radii equal to 15 Å, which usually gives 4–20 k-points depending on the sample size. The geometries were relaxed using the conjugate gradient method until all interatomic forces were smaller than 0.04 eV/Å and the total stress was less than 0.0005 eV/Å^3. No geometrical constrains were applied during relaxation.

C. GB structural model

It is common practice to generate GB by means of the coincidence site lattice (CSL) and this theory has also been used to study low-energy GB in graphene.[17] The CSL theory, however, includes only symmetric grain configurations and is not suitable to deal with generic GB, like the DBGB we study here. Therefore, we use a more general model, inspired by the theory of nanotubes[48] and similar to that used in Refs. 14 and 17 for symmetric GB.

A nanotube is uniquely defined by a pair of integers (m,n) relating the chirality vector $\mathbf{C}_h$ to the basis vectors of the hexagonal lattice $(\mathbf{a}_1,\mathbf{a}_2)$ as

$$\mathbf{C}_h = m\mathbf{a}_1 + n\mathbf{a}_2, \tag{1}$$

where

$$\mathbf{a}_1 = r_{cc}(-\sqrt{3}/2,3/2) \qquad \mathbf{a}_2 = r_{cc}(\sqrt{3}/2,3/2) \tag{2}$$

and $r_{cc} = 1.42$ Å is the interatomic distance in graphene giving $a_0 = \sqrt{3}r_{cc}$ as lattice constant [see Fig. 1(a)]. For nanotubes, the vector $\mathbf{T}$ orthogonal to $\mathbf{C}_h$ gives the nanotube axis and $\mathbf{C}_h$ gives the direction of rolling. In terms of (m,n) the vector $\mathbf{T}$ is given by

$$\mathbf{T} = \frac{t_1}{k}\mathbf{a}_1 + \frac{t_2}{k}\mathbf{a}_2, \tag{3}$$

where

$$t_1 = -m - 2n \qquad t_2 = 2m + n \tag{4}$$

and k is the greatest common divisor of $|t_1|$ and $|t_2|$.

Furthermore, we call $\mathbf{R}_A$ and $\mathbf{R}_B$ the positions of the two atoms in the unit cell of the hexagonal lattice. The case

$$\mathbf{R}_A = r_{cc}(0,1,0) \qquad \mathbf{R}_B = r_{cc}(0,2,0) \tag{5}$$

is illustrated in the unit cell shown in Fig. 1(b).

While for nanotubes the vectors $\mathbf{C}_h$ and $\mathbf{T}$ are used to define a rectangle of given chirality to be rolled, for GB the chirality vector $\mathbf{C}_h$ determines the direction of the grain boundary
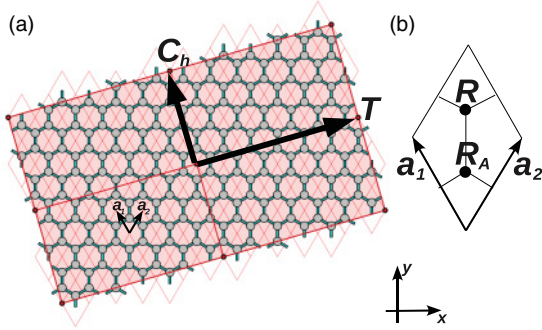
FIG. 1. (Color online) Definition of chirality vector (a) and unit cell (b). For clarity, the grain defined by vectors $\mathbf{C}_h$ and $\mathbf{T}$ is replicated twice along the direction of $\mathbf{C}_h$ and $\mathbf{T}$.

while the rectangular area is the graphene grain, as shown in Fig. 1(a). In the CSL approach the second grain is symmetric with respect to the GB direction given by $\mathbf{C}_h$.

The length $d(m,n)$ of $\mathbf{C}_h$ in our basis is

$$d(m,n) = r_{cc}\sqrt{3\Sigma}, \tag{6}$$

where

$$\Sigma = m^2 + mn + n^2. \tag{7}$$

There may be different pairs (m,n) that give the same value of Σ. For example $\Sigma = 91$ may be obtained by pairs $(1,9)$ and $(5,6)$ so, for $\Sigma = 91$, Eq. (7) has the four solutions $(1,9); (9,1); (5,6); (6,5)$.

The couples $(1,9); (9,1)$ and $(5,6); (6,5)$ are symmetric and are described by a single tilt angle in the CSL theory, whereas, e.g., the pair $(1,9); (5,6)$ is not symmetric and requires definition of the two misorientation angles of the two grains

$$\cos\phi_i = \frac{2m_i + n_i}{2\sqrt{m_i^2 + m_i n_i + n_i^2}} \quad i = 1,2. \tag{8}$$

In this way, by selecting two grains with the same Σ we can satisfy periodic boundary conditions also for nonsymmetric grains selecting different chirality vectors $\mathbf{C}_{h1}$ and $\mathbf{C}_{h2}$ together with the orthogonal vectors $\mathbf{T}_1$ and $\mathbf{T}_2$. This procedure allows to cut two rectangular grains with the same periodicity d that, after proper reorientation, can be joined together to form the GB, labeled now by two pairs of indexes (m_1,n_1) and (m_2,n_2). In case of symmetric grains, i.e., $n_1 = n_2$ and $m_1 = m_2$, we can define $\theta = \phi_1 + \phi_2$.

Since the two grains are rectangular, the final structure forms a rectangular unit cell that contains two grains with two GB. This construction gives us a starting point for the search of metastable nonsymmetric GB that we describe in the next section.

D. Search of (meta-)stable DBGB

Once the procedure for building GB considers also asymmetric grains, most situations will yield structures with large strain and atoms that are too close to each other, from 1.5 Å to 0.1 Å or even less. We have used two parameters to help the search for favorable structures. First, we introduce the

parameter $r_{\min}$ which controls the minimal distance between atoms. If two atoms are closer than $r_{\min}$, then this pair is replaced by a single atom with average coordinates. The parameter $r_{\min}$ influences the density of atoms along the grain boundary. We have searched with different values, namely $r_{\min} = 0.1, 0.4, 1.2$ Å. This procedure is physically justified because, in the situation of crystal growth at high temperatures, carbon atoms would be redistributed in such a way as to avoid too-close overlap of the atomic cores. The other free parameter in our scheme is the shift $\mathbf{r}_{sh}$ of the sublattice vectors $\mathbf{R}_A$ and $\mathbf{R}_B$,

$$\mathbf{R}_A = \mathbf{r}_{sh} + r_{cc}(0,0,0) \qquad \mathbf{R}_B = \mathbf{r}_{sh} + r_{cc}(0,1,0). \tag{9}$$

We use two values,

$$\mathbf{r}_{sh}^1 = r_{cc}(0,0,0) \qquad \mathbf{r}_{sh}^2 = r_{cc}(0,1,0), \tag{10}$$

where $\mathbf{r}_{sh}^1$ puts the origin of the cell on one atom and $\mathbf{r}_{sh}^2$ gives the $\mathbf{R}_A$ and $\mathbf{R}_B$ shown in Fig. 1.

We use the freedom given by the procedure described above to construct thousands of initial configurations with GB. For each configuration, we optimize the structure by annealing the sample from 3300 K by Monte Carlo simulations in the NPT ensemble with the LCBOPII interatomic potential. After a large number of Monte Carlo moves, we find structures that no longer evolve and can be considered as metastable. Among all these configurations we search automatically the ones with twofold coordinated carbon atoms.

Among these possibilities, the structure with 5-8-7 rings (see Fig. 3) is the simplest and most common. Therefore, we have concentrated on this structure as prototype of DBGB. For simplicity, we have then constructed samples with 5-8-7
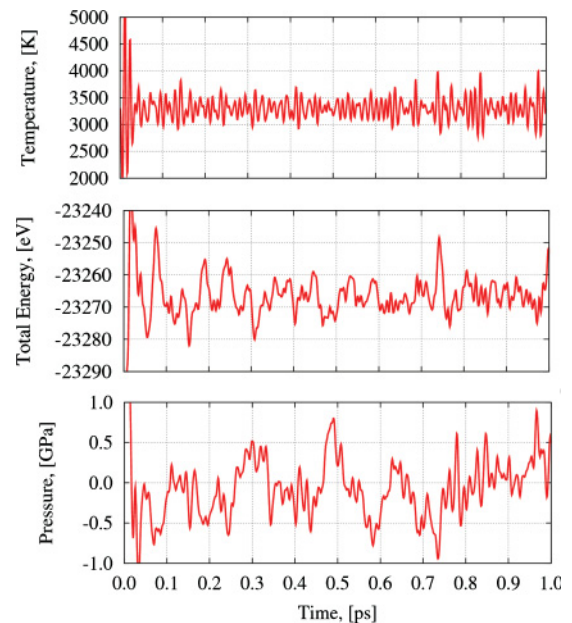

FIG. 2. (Color online) Time dependence of temperature T, total energy E_T, and pressure (total stress) P during 1000 steps of MD annealing for a sample with GB with two 5-8-7 defects and 150 atoms. The mean values are $M(T) = 3299.39$ K, $M(E_T) = -23\,266.89$ eV, $M(P) = -0.056$ GPa with standard deviation $\sigma(T) = 187.64$ K, $\sigma(E_T) = 4.80$ eV, $\sigma(P) = 0.327$ GPa and correlation $\rho(T,E_T) = 0.039$, $\rho(P,E_T) = -0.247$, $\rho(T,P) = 0.177$.

DBGB and different periods with symmetric grains defined by (m,n) and θ. Further relaxation of the selected structure with SIESTA affects the structure of graphene GB only marginally, which confirms the accuracy of our atomistic energy minimization. Last, we calculate electronic and magnetic properties with SIESTA.

We have checked the stability of the 5-8-7 DBGB also by performing constant-temperature molecular dynamics (MD) with Nose thermostat using the DFT package SIESTA at 3300 K with a time step of 1 fs. The time dependence of temperature, energy, and pressure are shown in Fig. 2. After 1000 MD steps the structure of the 5-8-7 defect keeps its original geometry. During the dynamics, however, we observe an exchange of a six-ring with a seven-ring that causes a mirror reflection of the 5-8-7 point defect with respect to the GB line. This transformation, which retains the original structure of the twofold coordinated atom, is shown in Fig. 5(d).

III. STRUCTURE AND ENERGETICS OF DBGB IN GRAPHENE

A more general way of describing GB is to present them as arrays of dislocations.[49] Low-energy symmetric GB are nothing but arrays of 5-7 (glide) dislocations. The DBGB that we select in our search for metastable structures contain more complicated structural elements characterized by the presence of eight-, nine-, and fourfold rings. These rings appear also

in simulations of disordered graphene[16] and graphene at high temperatures[50] and were experimentally observed in electron-bombarded graphene.[22]

In Ref. 51 another type of dislocation, the shuffle dislocation shown in Fig. 4, with one eightfold ring with one dangling bond, has been proposed as a potential carrier of a magnetic moment. In our search for metastable structures with dangling bonds, we have found eightfold rings only in combination with other nonhexagonal rings. If we construct an eight-ring shuffle dislocation we find that above 2400 K it transforms to a 5-8-7 configuration (these two dislocation configurations are characterized by the same Burgers vector, as will be discussed in detail below). By looking at Figs. 3 and 4 one can see that the shuffle GB (i.e., the wall of shuffle dislocations) has the largest out-of-plane distortion, which increases the strain in the structure[17] and might explain its instability.

In our Monte Carlo simulations at 3300 K, we find most frequently the sequence 5-8-7, which has one twofold coordinated carbon atom. This atom has one unpaired electron and, as a result, is the source of magnetic moment. We call this atom, therefore, a magnetic atom. If we remove the magnetic atom and apply further relaxation, we find the nonmagnetic 5-7 defect. In Fig. 5 we show how the 5-8-7 is related to the 5-7 defect and how it can be constructed by either adding [Fig. 5(b)] or removing [Fig. 5(a)] an atom from it. The similar construction of a shuffle defect is shown in Fig. 5(c). This procedure is technically reversible so a 5-7 can be obtained by
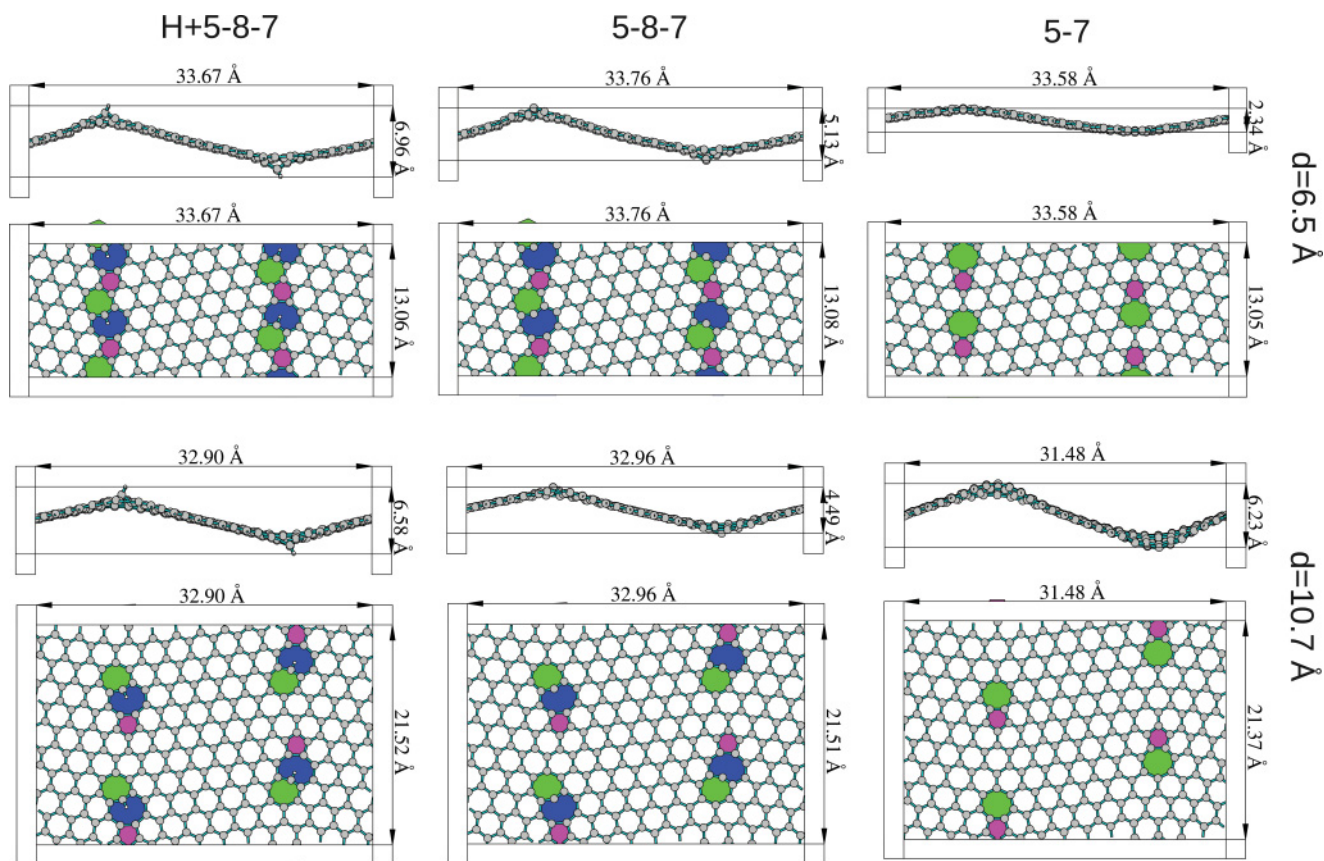

FIG. 3. (Color online) Side and top view of (from top to bottom) 5-7, 5-8-7, H+5-8-7 GB for two values of the period d, (left) $d = 6.5$ Å and (right) $d = 10.7$ Å. The unit cell is replicated twice in the GB direction. For clarity, seven-rings are green (light gray), five-rings are pink (gray), and eight-rings are blue (black).
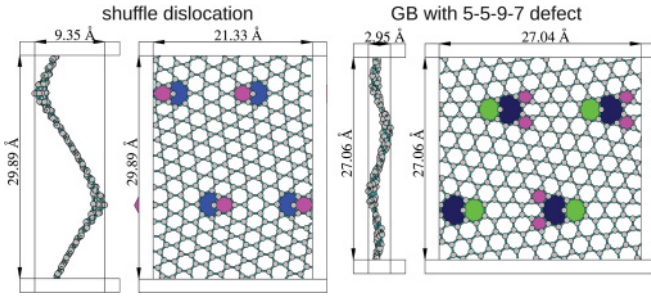
FIG. 4. (Color online) Side and top view of shuffle (left) and 5-5-9-7 GB. The unit cell is replicated twice in the GB direction. For clarity, in the shuffle GB we color also the six-ring.

removing the magnetic atom and letting the structure rebound and relax.

One could expect the 5-8-7 DBGB to have the same Burgers vector of the glide and shuffle dislocation. In fact, if we consider the dislocation as a disclination dipole[49] the Burgers vector **b** is the product of the Frank vector of the disclination times the dipole arm. If we double the distance between the five- and sevenfold rings that constitute the disclination, we could expect a twice larger Burgers vector $\mathbf{b} \to 2\mathbf{b}$. The eightfold ring between the five- and sevenfold rings can be considered as a shuffle dislocations with Burgers vector $-\mathbf{b}$ so the resulting Burgers vector is $2\mathbf{b} - \mathbf{b} = \mathbf{b}$.

This analysis is supported by the data shown in Table I where we compare GB made of arrays of the 5-7 and 5-8-7 disclination dipoles shown in Fig. 3. The Burgers vector was calculated using the Frank equation[49]

$$b = 2d \sin \theta / 2, \quad (11)$$

where d is the periodicity of the array and θ is the misorientation angle. One can, indeed, see that the Burgers vector of the 5-7 and 5-8-7 are almost the same. We also compare the formation energy of defects E_F calculated as

$$E_F = \left(E_{\text{Total}}^{\text{Defect}} - E_{\text{Total}}^{\text{Graphene}} \frac{N_{\text{atoms}}^{\text{Defect}}}{N_{\text{atoms}}^{\text{Graphene}}} \right) \bigg/ N_{\text{Defects}} \quad (12)$$
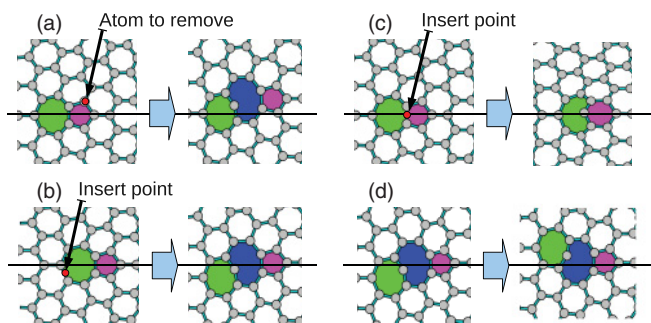

FIG. 5. (Color online) The 5-7 and 5-8-7 defects are related geometrically. There are two ways to construct a 5-8-7 defect from 5-7: remove an atom from pentagon (a) and insert an adatom to the bond belonging to heptagon (b). In the same way, we can construct a shuffle dislocation from 5-7 (c). In panel (d) we show the mirror transformation of the 5-8-7 observed in the MD simulations at $T = 3300$ K described in Sec. II D.

TABLE I. Summary of the studied defects with GB period d, Burgers vector **b**, GB formation energy E_F, and hydrogen adsorption energy (with respect to the hydrogen atom) E_{ads}. The tilt angle together with Burgers vector were calculated for z-projected geometries, i.e., completely flat samples with $z = 0$. The binding energy of the hydrogen molecule in the used model is $E_{H_2} = 4.53$ eV.

GB	GB period d (Å)	Tilt angle θ°	Burgers vector **b** (Å)	E_F (eV/defect)
5-7	6.52	20.8	2.360	2.31
5-8-7	6.54	21.7	2.467	6.83
H+5-8-7	6.53	21.7	2.461	$E_{\text{ads}} = 4.78$
5-7	10.69	13.7	2.544	3.87
5-8-7	10.76	12.7	2.378	8.01
H+5-8-7	10.76	12.5	2.350	$E_{\text{ads}} = 4.60$
Shuffle	10.66	13.2	2.451	8.16
5-5-9-7	13.59	17.7	4.185	8.63

for different types of GB. The formation energy of the 5-8-7 GB is approximately twice the one of the 5-7 for the same periodicity, which is not surprising since the dangling bond costs some additional energy. The larger formation energy for the larger periodicity is consistent with the finding[17] that dislocation cores attract each other, contrary to three-dimensional materials.

The presence of the dangling bond makes bonding to other species possible. We also have, therefore, studied the 5-8-7 when the magnetic atom is bound to a hydrogen atom, a structure we call H+5-8-7, or to an oxygen atom or OH group, which we call O+5-8-7 and OH+5-8-7, respectively. The top and side views of H+5-8-7 shown in Fig. 3 do not differ much from those of the 5-8-7. Only the local structure of the magnetic atom is somewhat changed. In particular, the bonds to its two carbon neighbors go from ~1.37 Å in 5-8-7 to ~1.41 Å in H+5-8-7, a value closer to the bulk value 1.42 Å. The angle between these two bonds is also changed. The rest of the structure remains basically the same as shown in Fig. 6 also for the case of oxygen and OH.

It is remarkable that the adsorption energy of the H+5-8-7 is just a bit higher than the H_2 binding energy calculated within the same method. This means that, within our computational scheme, the hydrogenation of DBGB is energetically favorable. At the same time, the difference is small and one should take into account that the density functional within GGA underestimates strongly the binding energy of H_2 molecule. Fortunately, the issue of the hydrogenation does not affect qualitatively our conclusions about the structure (as it is shown here) and magnetism (as will be shown below) of DBGB.

Since the 5-8-7 DBGB has minimal Burgers vector and low strain in view of its flatness it is natural to assume that it has the lowest energy among DBGB and, therefore, represents the most natural candidate as source of magnetism in GB. That is why we will focus on this structural element in the rest of our paper. Of course, more complicated DBGB exist and, as an example, we show in Fig. 4 the structure of a GB with $\theta = 17.7°$ formed by a periodic array of a 5-5-9-7 structural element. As reported in Table I, this GB has formation energy
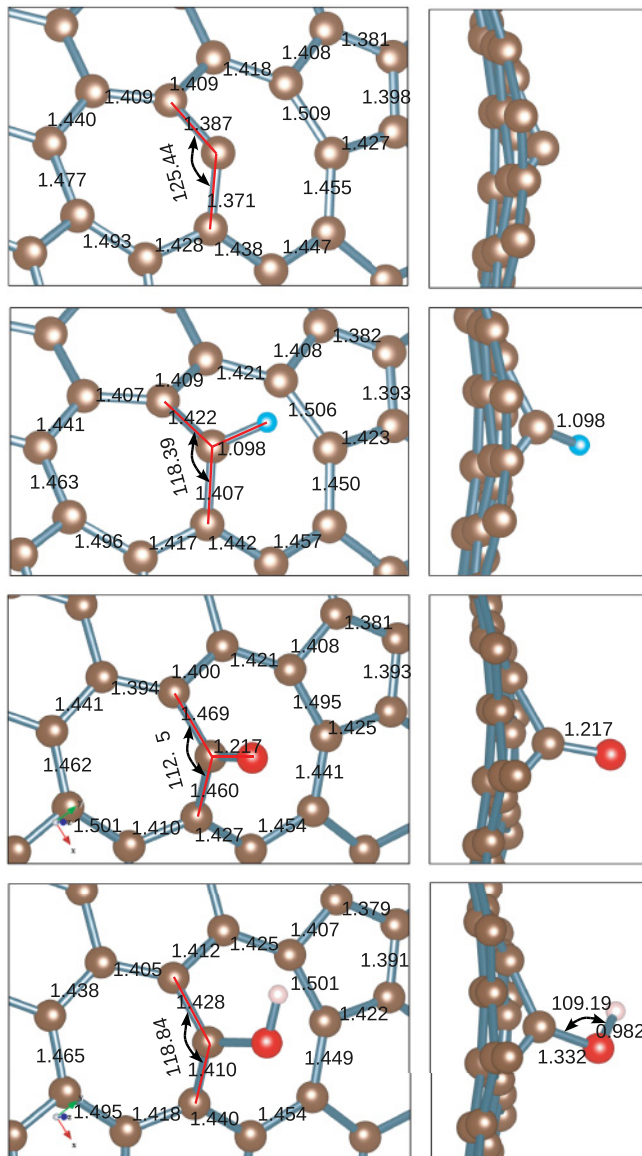
FIG. 6. (Color online) Bond lengths and C-C-C angle of magnetic atom for (from top to bottom) 5-8-7, H+5-8-7, O+5-8-7, OH+5-8-7 DBGB.

FIG. 7. (Color online) p_x, p_y, and p_z components of total DOS for 5-8-7 and H+5-8-7 DBGB with misorientation angle $\theta = 21.7°$. Red solid and dashed green curves are for spin up and spin down, respectively.

p_z and essentially differs for spin up and spin down. For the H+5-8-7 there is even an almost half-metallic situation with the Fermi energy lying just below the gap for majority spin electron states. Below the Fermi energy but relatively far from it, there is also a smaller gap for minority electron states. The tiny p_x, p_y components are related to the distortion from a planar sp^2 bond. In Table II we report the magnetic moments per magnetic atom. They are, in general, not integers. Importantly, hydrogen adsorption does not destroy the magnetic moment. This is because the magnetic atom is not like a usual dangling bond that can be fully saturated by hydrogen. A carbon atom participates with three electrons to in-plane bonding and with the fourth to the p_z band. Therefore,

just slightly higher than the 5-8-7 and an almost double Burgers vector. The latter statement is justified by taking into account the change of type of GB from zigzag to armchair.[14] In the following section, we examine in detail the 5-8-7 in comparison to the 5-7.

IV. ELECTRONIC STRUCTURE AND SPIN DENSITY OF DBGB IN GRAPHENE

We have calculated the spin-polarized density of states (DOS) of selected DBGB by means of SIESTA. We project the states onto the orbitals representing the p_x, p_y, and p_z. In Appendix we validate our approach against previous results for the H-saturated zigzag graphene edges[52,53] while comparing them to nonsaturated edges. In Fig. 7 we present the spin-polarized DOS for ferromagnetically oriented magnetic moments associated to the dangling bond of a 5-8-7 and H+5-8-7 with period $d = 6.5$ Å. We see that DOS is mostly
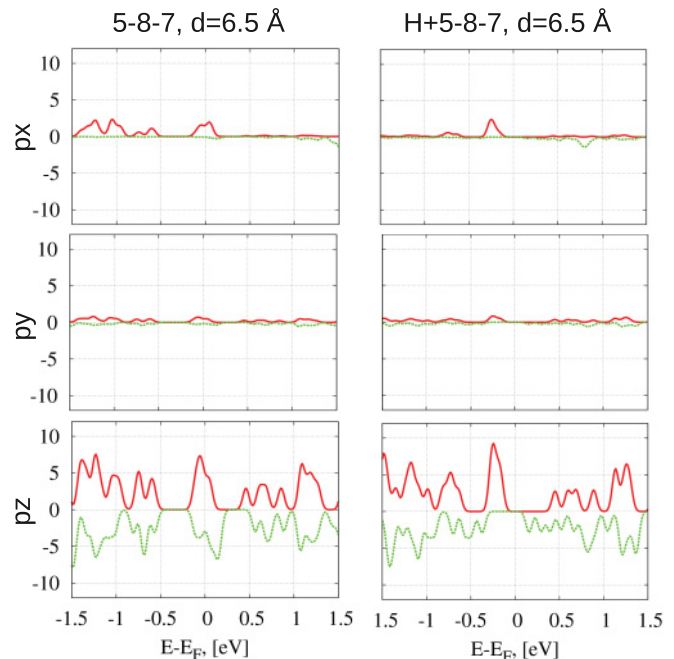
TABLE II. Magnetic moment contribution in μ_B from magnetic atom which carries dangling bond (DB atom) for the studied samples with two GB and one magnetic defect per GB.

| System	From DB atom	Number of DB atoms	From non-DB atoms	From whole system
H+5-8-7 $d = 6.5$ (Å)	0.530	2	0.956	2.001
5-8-7 $d = 6.5$ (Å)	0.933	2	0.843	2.708
H+5-8-7 flat $d = 6.5$ (Å)	0.496	2	1.019	1.997
5-8-7 flat $d = 6.5$ (Å)	0.921	2	0.850	2.692
OH+5-8-7 $d = 10.7$ (Å)	0.291	2	0.468	1.068
H+5-8-7 $d = 10.7$ (Å)	0.542	2	0.895	1.963
5-8-7 $d = 10.7$ (Å)	0.455	2	−0.742	0.169
H+5-8-7 flat $d = 10.7$ (Å)	0.455	2	1.037	1.933
5-8-7 flat $d = 10.7$ (Å)	0.987	2	0.990	2.964
Shuffle $d = 10.7$ (Å)	0.424	2	−0.011	0.837
5-5-9-7 $d = 13.6$ (Å)	0.889	2	−0.333	1.445
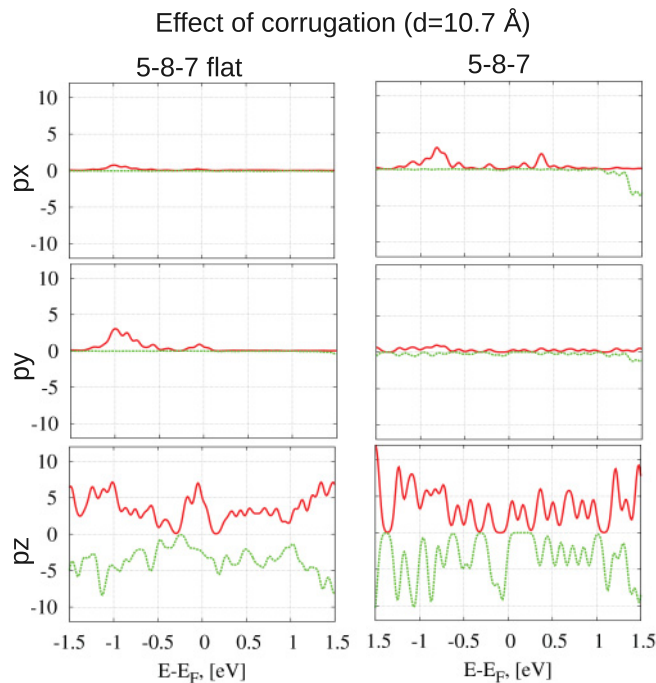
FIG. 8. (Color online) The effect of corrugation on the DOS (see the text) is seen by comparing the minimal energy 5-8-7 DBGB with the flat one. Red solid and dashed green curves are for spin up and spin down, respectively.

the twofold coordination in the plane provides a dangling bond that adds to and distorts the p_z orbital. The OH group reduces further the magnetic moment, whereas oxygen destroys it completely.

Last, we have found that the out-of-plane corrugation affects the magnetic moment of the 5-8-7 while it is not important for the H+5-8-7. In principle, this effect can be used to control magnetic moments through strain and, therefore, it deserves a more detailed discussion. To this aim, in Fig. 8 we compare the DOS of the 5-8-7 with the one obtained for the same structure without allowing out-of-plane distortions, namely for a flat 5-8-7. Since the out-of-plane corrugation is larger for $d = 10.7$ Å (see Fig. 3), we have chosen this case to illustrate this effect. One can see that the DOS essentially differs for the cases with and without out-of-plane deformations. The different DOS are also reflected in the almost double value of the magnetic moments of the flat 5-8-7 as reported in Table II. Conversely, the magnetic moments of relaxed and flat H+5-8-7 are comparable.

To understand the origin of this effect we have studied the spin density in the system. In Figs. 9 and 10 we use two representations of the spin density. The one to the right is the most common representation of isosurfaces of the spin density. The representation to the left gives the amount of spin per atom obtained from Mullikan population analysis represented as a sphere of radius proportional to the logarithm of the spin. This representation makes it possible to visualize also the small spin-density components. In this way one can see that the up and down components away from the defect seem to be located on the A and B sublattices of graphene. This alternation is broken by the defect in a way that depends on the out-of-plane
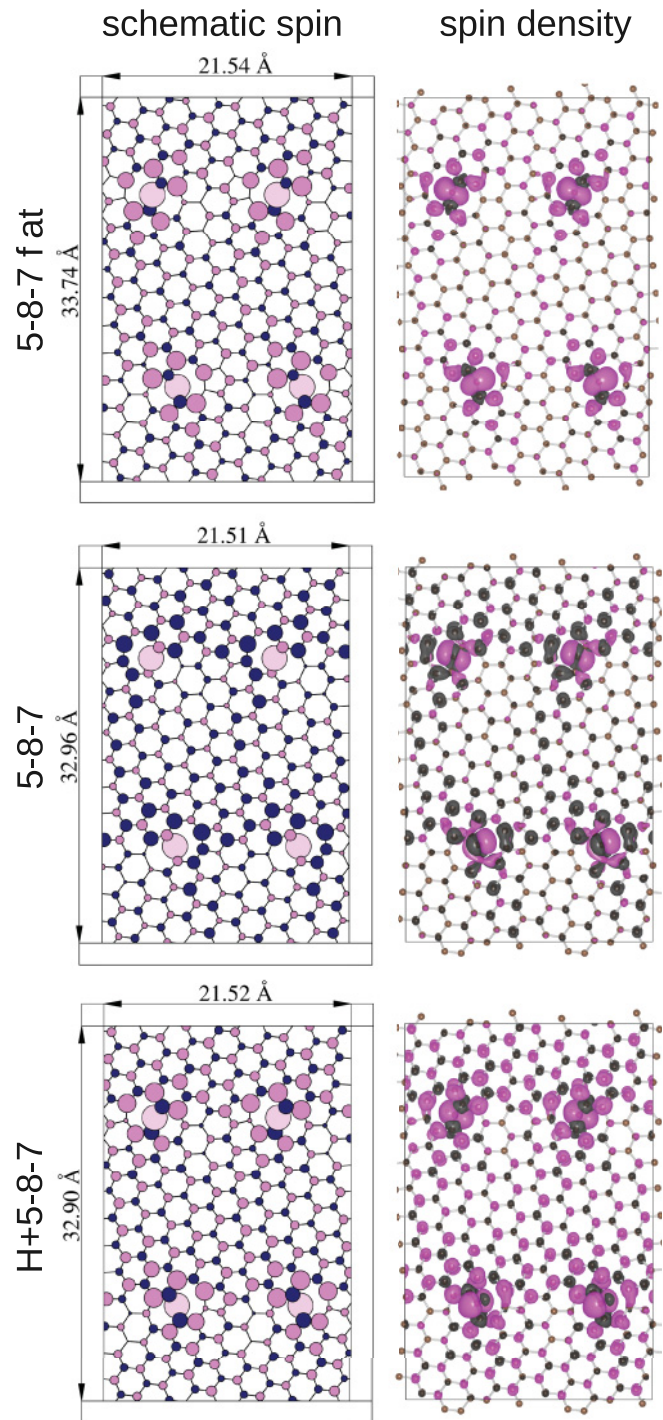

FIG. 9. (Color online) Right panels: isosurface plot of the spin density for the 5-8-7 DBGB with $\theta = 12.7°$. Left panels: symbolic representation of the spins per atom (see text). Pink (gray) and blue (dark gray) represent spin up and spin down, respectively. In the left panels the magnetic atoms are light pink (light gray). From top to bottom: flat configuration; minimum energy configuration without hydrogen; minimum energy configuration with hydrogen.

distortions. In fact, in the flat 5-8-7, the magnetic atom (light gray) with spin up has the two nearest neighbors of spin down, whereas, in the relaxed 5-8-7, the nearest neighbors have the same spin up of the magnetic atom.
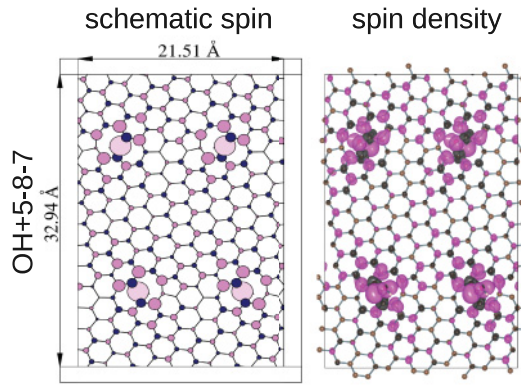
FIG. 10. (Color online) Right panel: isosurface plot of the spin density for the OH+5-8-7 DBGB with $\theta = 12.7°$. Left panel: symbolic representation of the spins per atom (see text). Pink (gray) and blue (dark gray) represent spin up and spin down, respectively. In the left panels the magnetic atoms are light pink (light gray).

The H+5-8-7 is not sensitive to the corrugation and the spin distribution for the flat case is very similar to the one shown for the relaxed H+587 in Fig. 9.

V. CONCLUSIONS

Grain boundaries seem to be unavoidable structural elements of large-enough graphene samples, irrespective of their preparation. By analogy with conventional three-dimensional material science, one may expect that they will affect strongly both the mechanical and electronic properties of graphene. From a theoretical point of view, GB are very complicated

objects due to the multiscale character of the problem. Both long-range deformations extending over tens of thousands of atoms and specific atomistic and electronic structure of the cores are essential. Therefore, usually people study only special GB, mostly those which can be constructed by the CSL approach.[14,17] These GB are, indeed, usually the most energetically favorable. At the same time, e.g., for CVD growth of graphene on metals,[6,7] one could expect that various crystallites grow independently from many centers and more complicated GB will be formed. To attack this problem we have combined large-scale atomistic simulations using the LCBOBII potential[28] with *ab initio* calculations. We have studied in detail GB containing the 5-8-7 defect, which is the carrier of the magnetic moment. Based on the results presented here one can conclude that a generic GB should contain magnetic moments that are robust enough, in particular, with respect to hydrogenation. Since GB in graphene are one-dimensional objects, they cannot lead to magnetic ordering at any finite temperature. We have shown, however, that the very existence of magnetic moments at the GB dangling bonds modifies the local electronic structure around the Fermi energy that can be probed by STM.
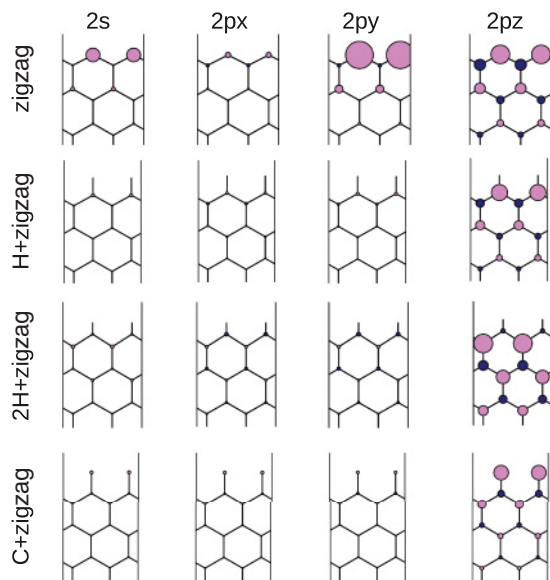
FIG. 11. (Color online) Zigzag, single hydrogenated zigzag, double hydrogenated zigzag, and model zigzag graphene edge with carbon. For each case the magnetic moment decomposition over atomic orbitals for carbon atoms only is shown according to Mulliken atomic orbital population analysis. The square of each circle is proportional to the value of magnetic moment contribution. Pink (light gray) and blue (dark gray) are positive and negative values of spin, respectively.

APPENDIX: VALIDATION TEST FOR MAGNETISM OF ZIGZAG GRAPHENE EDGE WITH AND WITHOUT HYDROGENATION

To check our computational scheme we have carried out electronic structure calculations for two cases where graphene is supposed to be magnetic, namely zigzag edges[52,53] with and without passivation by single- and double hydrogen and carbon-terminated zigzag edge (see Fig. 11). The results are shown in Table III. One can see that in all cases we have excellent agreement with previous results. Furthermore, we present, in Table IV, more detailed information about the orbital contributions to the magnetic moments.

TABLE III. Magnetic moment contribution in μ_B from A and B sublattices for four studied cases.

System	m_A	m_B	$m_A + m_B$	with H	$m_A + m_B$
zz	1.464	−0.154	1.310	–	1.29 from[53]
H+zz	0.453	−0.134	0.330	0.310	0.30 from[52]
2H+zz	−0.233	0.738	0.505	0.625	–
C+zz	−0.080	0.390	0.310	–	–

TABLE IV. Detailed information about distribution of magnetic moment over orbitals for onefold (1nn), twofold (2nn), threefold (3nn) coordinated edge carbon atoms in the four different systems shown in Fig. 11, i.e., zz for zigzag, H+zz for single hydrogenated zigzag, 2H+zz for double hydrogenated zigzag, and C+zz for model zigzag graphene edge with carbon atom at the edge

C atom	$2s$	$2px$	$2py$	$2pz$	all-d	sum
zz 2nn	0.176	0.026	0.691	0.320	−0.009	1.206
zz 3nn	0.002	−0.010	−0.012	−0.112	0.075	−0.060
H+zz 2nn	0.001	0.007	0.010	0.266	−0.002	0.290
H+zz 3nn	0.002	−0.008	−0.006	−0.071	0.025	−0.057
2H+zz 2nn	−0.004	−0.013	−0.015	−0.019	0.036	−0.017
2H+zz 3nn	0.012	0.008	0.010	0.345	0.000	0.375
C+zz 1nn	0.010	0.011	0.009	0.226	0.002	0.256
C+zz 2nn	0.004	−0.004	−0.007	−0.048	0.018	−0.038
C+zz 3nn	0.002	0.002	0.000	0.074	−0.003	0.075

[1] C. Berger, Z. Song, T. Li, X. Li, A. Y. Ogbazghi, R. Feng, Z. Dai, A. N. Marchenkov, E. H. Conrad, P. N. First, and W. A. de Heer, J. Phys. Chem. B **108**, 19912 (2004).

[2] C. Berger, Z. Song, X. Li, X. Wu, N. Brown, C. Naud, D. Mayou, T. Li, J. Hass, A. N. Marchenkov, E. H. Conrad, P. N. First, and W. A. de Heer, Science **312**, 1191 (2006).

[3] P. Blake, P. D. Brimicombe, R. R. Nair, T. J. Booth, D. Jiang, F. Schedin, L. A. Ponomarenko, S. V. Morozov, H. F. Gleeson, E. W. Hill, A. K. Geim, and K. S. Novoselov, Nano Lett. **8**, 1704 (2008).

[4] Y. Hernandez, V. Nicolosi, M. Lotya, F. M. Blighe, Z. Sun, S. De, M. T., B. Holland, M. Byrne, Y. K. Gun'Ko, J. J. Boland, P. Niraj, G. Duesberg, S. Krishnamurthy, R. Goodhue, J. Hutchison, V. Scardaci, A. C. Ferrari, and J. N. Coleman, Nat. Nanotechnol. **3**, 563 (2008).

[5] M. Choucair, P. Thordarson, and J. A. Stride, Nat. Nanotechnol. **4**, 30 (2009).

[6] X. Li, W. Cai, J. An, S. Kim, J. Nah, D. Yang, R. Piner, A. Velamakanni, I. Jung, E. Tutuc, S. K. Banerjee, L. Colombo, and R. S. Ruoff, Science **324**, 1312 (2009).

[7] S. Bae, H. Kim, Y. Lee, X. Xu, J.-S. Park, Y. Zheng, J. Balakrishnan, T. Lei, H. Ri Kim, Y. I. Song, Y.-J. Kim, K. S. Kim, B. Ozyilmaz, J.-H. Ahn, B. H. Hong, and S. Iijima, Nat. Nanotechnol. **5**, 574 (2010).

[8] D. L. Miller, K. D. Kubista, G. M. Rutter, M. Ruan, W. A. de Heer, P. N. First, and J. A. Stroscio, Science **324**, 924 (2009).

[9] J. Coraux, A. T. N'Diaye, C. Busse, and T. Michely, Nano Lett. **8**, 565 (2008).

[10] E. Loginova, S. Nie, K. Thürmer, N. C. Bartelt, and K. F. McCarty, Phys. Rev. B **80**, 085430 (2009).

[11] H. J. Park, J. Meyer, S. Roth, and V. Skakalova, Carbon **48**, 1088 (2010).

[12] P. Y. Huang, C. S. Ruiz-Vargas, A. M. van der Zande, W. S. Whitney, M. P. Levendorf, J. W. Kevek, S. Garg, J. S. Alden, C. J. Hustedt, Y. Zhu, J. Park, P. L. McEuen, and D. A. Muller, Nature **469**, 389 (2011).

[13] J. Lahiri, Y. Lin, P. Bozkurt, I. I. Oleynik, and M. Batzill, Nat. Nanotechnol. **5**, 326 (2010).

[14] O. V. Yazyev and S. G. Louie, Phys. Rev. B **81**, 195420 (2010).

[15] R. Grantab, V. B. Shenoy, and R. S. Ruoff, Science **330**, 946 (2010).

[16] S. Malola, H. Häkkinen, and P. Koskinen, Phys. Rev. B **81**, 165447 (2010).

[17] J. M. Carlsson, L. M. Ghiringhelli, and A. Fasolino, Phys. Rev. B **84**, 165423 (2011).

[18] O. V. Yazyev and S. G. Louie, Nat. Mater. **9**, 806 (2010).

[19] M. L. Kronberg and F. H. Wilson, J. Met. **185**, 501 (1949).

[20] R. Z. Valiev, R. K. Islamgaliev, and I. V. Alexandrov, Prog. Mater. Sci. **45**, 103 (2000).

[21] A. Mesaros, S. Papanikolaou, C. F. J. Flipse, D. Sadri, and J. Zaanen, Phys. Rev. B **82**, 205119 (2010).

[22] J. Kotakoski, A. V. Krasheninnikov, U. Kaiser, and J. C. Meyer, Phys. Rev. Lett. **106**, 105505 (2011).

[23] O. V. Yazyev, Rep. Prog. Phys. **73**, 056501 (2010).

[24] J. Cervenka, M. I. Katsnelson, and C. F. J. Flipse, Nat. Phys. **5**, 840 (2009).

[25] D. Martínez-Martín, M. Jaafar, R. Pérez, J. Gómez-Herrero, and A. Asenjo, Phys. Rev. Lett. **105**, 257203 (2010).

[26] M. Sepioni, R. R. Nair, I-Ling Tsai, A. K. Geim, and I. V. Grigorieva, Europhys. Lett. **97**, 47001 (2012).

[27] D. M. Edwards and M. I. Katsnelson, J. Phys. Condens. Matter **18**, 7209 (2006).

[28] J. H. Los, L. M. Ghiringhelli, E. J. Meijer, and A. Fasolino, Phys. Rev. B **72**, 214102 (2005).

[29] [http://sourceforge.net/projects/xyz2eps/].

[30] PYTHON software foundation, PYTHON programming language, version 2.6.5 http://www.python.org/.

[31] K. Momma and F. Izumi, J. Appl. Crystallogr. **41**, 653 (2008).

[32] A. Fasolino, J. H. Los, and M. I. Katsnelson, Nat. Mater. **6**, 858 (2007).

[33] J. H. Los, M. I. Katsnelson, O. V. Yazyev, K. V. Zakharchenko, and A. Fasolino, Phys. Rev. B **80**, 121405 (2009).

[34] K. V. Zakharchenko, M. I. Katsnelson, and A. Fasolino, Phys. Rev. Lett. **102**, 046808 (2009).

[35] L. J. Karssemeijer and A. Fasolino, Surf. Sci. **605**, 1611 (2011).

[36] J. M. H. Kroes, M. A. Akhukov, J. H. Los, N. Pineau, and A. Fasolino, Phys. Rev. B **83**, 165411 (2011).

[37]K. V. Zakharchenko, J. H. Los, M. I. Katsnelson, and A. Fasolino, Phys. Rev. B **81**, 235439 (2010).

[38]P. Hohenberg and W. Kohn, Phys. Rev. **136**, B864 (1964).

[39]W. Kohn and L. J. Sham, Phys. Rev. **140**, A1133 (1965).

[40]J. M. Soler, E. Artacho, J. D. Gale, A. Garcia, J. Junquera, P. Ordejon, and D. Sanchez-Portal, J. Phys. Condens. Matter **14**, 2745 (2002).

[41]D. Sanchez-Portal, P. Ordejon, and E. Canadell, *Principles and Applications of Density functional Theory in Inorganic Chemistry II* Vol. 113 (Springer, Berlin, 2004), pp. 103–170.

[42]E. Artacho, E. Anglada, O. Dieguez, J. D. Gale, A. Garcia, J. Junquera, R. M. Martin, P. Ordejon, J. M. Pruneda, D. Sanchez-Portal, and J. M. Soler, J. Phys. Condens. Matter **20**, 064208 (2008).

[43]J. P. Perdew, K. Burke, and M. Ernzerhof, Phys. Rev. Lett. **77**, 3865 (1996).

[44]J. Junquera, O. Paz, D. Sánchez-Portal, and E. Artacho, Phys. Rev. B **64**, 235111 (2001).

[45]N. Troullier and J. L. Martins, Phys. Rev. B **43**, 1993 (1991).

[46]L. Kleinman and D. M. Bylander, Phys. Rev. Lett. **48**, 1425 (1982).

[47]H. J. Monkhorst and J. D. Pack, Phys. Rev. B **13**, 5188 (1976).

[48]R. Saito, G. Dresselhaus, and M. S. Dresselhaus, *Physical Properties of Carbon Nanotubes* (Imperial College Press, London, 1988).

[49]J. Hirth and J. Lothe, *Theory of Dislocations* (Wiley, New York, 1982), p. 870.

[50]K. V. Zakharchenko, A. Fasolino, J. H. Los, and M. I. Katsnelson, J. Phys. Condens. Matter **23**, 202202 (2011).

[51]M. P. López-Sancho, F. de Juan, and M. A. H. Vozmediano, Phys. Rev. B **79**, 075413 (2009).

[52]O. V. Yazyev and M. I. Katsnelson, Phys. Rev. Lett. **100**, 047209 (2008).

[53]S. Bhandary, O. Eriksson, B. Sanyal, and M. I. Katsnelson, Phys. Rev. B **82**, 165405 (2010).